AGU PUBLICATIONS

Geophysical Research Letters

RESEARCH LETTER
10.1002/2015GL064816

**Key Points:**
- Piled-up coronal mass ejection caused unexpectedly large major magnetic storm
- High-speed stream from coronal hole prevents the expansion of the ejecta from the behind
- Planar magnetic structures were found in the highly compressed sheath region

**Supporting Information:**
- Movie S1
- Figures S1 and S2

**Correspondence to:**
R. Kataoka,
kataoka.ryuho@nipr.ac.jp

**Citation:**
Kataoka, R., D. Shiota, E. Kilpua, and K. Keika (2015), Pileup accident hypothesis of magnetic storm on 17 March 2015, *Geophys. Res. Lett.*, *42*, 5155–5161, doi:10.1002/2015GL064816.

Received 3 JUN 2015
Accepted 24 JUN 2015
Accepted article online 25 JUN 2015
Published online 14 JUL 2015



# Pileup accident hypothesis of magnetic storm on 17 March 2015

**Ryuho Kataoka[1,2], Daikou Shiota[3], Emilia Kilpua[4], and Kunihiro Keika[3]**

[1]National Institute of Polar Research, Tachikawa, Japan, [2]Department of Polar Science, SOKENDAI (Graduate University for Advanced Studies), Tachikawa, Japan, [3]Solar-Terrestrial Environment Laboratory, Nagoya University, Nagoya, Japan, [4]Department of Physics, University of Helsinki, Helsinki, Finland

**Abstract** We propose a "pileup accident" hypothesis, based on the solar wind data analysis and magnetohydrodynamics modeling, to explain unexpectedly geoeffective solar wind structure which caused the largest magnetic storm so far during the solar cycle 24 on 17 March 2015: First, a fast coronal mass ejection with strong southward magnetic fields both in the sheath and in the ejecta was followed by a high-speed stream from a nearby coronal hole. This combination resulted in less adiabatic expansion than usual to keep the high speed, strong magnetic field, and high density within the coronal mass ejection. Second, preceding slow and high-density solar wind was piled up ahead of the coronal mass ejection just before the arrival at the Earth to further enhance its magnetic field and density. Finally, the enhanced solar wind speed, magnetic field, and density worked all together to drive the major magnetic storm.

## 1. Introduction

The largest magnetic storm so far during the solar cycle 24 occurred on 17 March 2015 with the minimum (provisional) *Dst* index of −223 nT at 2300 UT. Spectacular auroral displays were reported worldwide. For instance, northern lights were observed from Hokkaido, Japan, to the north in the morning sector at 1500–1700 UT on 17 March 2015, which was of high public interest because the last opportunity was more than 10 years ago on 8 November 2004 when the peak *Dst* index was −374 nT. GOES satellites observed geosynchronous magnetopause crossings at the same time at 1500–1700 UT due to the strong compression of the magnetosphere. The storm main phase had two-step development [*Kamide et al.*, 1998]. A halo coronal mass ejection (CME) associated with a C9.1 flare at 0200 UT on 15 March 2015 was the main driver of the storm, while the shock and the sheath region also played an additional role to cause the sudden commencement and the first step of the main phase, respectively. The CME was followed by a high-speed stream, which caused large enhancement of radiation belt electrons ($>10^4$ PFU/(cm$^2$ s sr) of >2 MeV electrons at GOES satellites) in the storm recovery phase.

The large magnetic storm was somewhat surprising for many specialists, and the space weather forecasters did not expect such an extraordinary high impact on the magnetosphere, e.g., according to Daily Reports of NOAA Space Weather Product. The halo CME was estimated to give only a glancing impact to the Earth, and it was associated with a relatively weak (C9.1) flare. The purpose of this study is to propose a "pileup accident" hypothesis to explain the formation mechanism of the unexpectedly geoeffective solar wind structure, to clarify the predictability for future space weather forecast.

## 2. Geoeffective Solar Wind Structure

The solar wind profile as obtained from the OMNI database is shown in Figure 1. An interplanetary shock was observed at 0430 UT, as identified by the rapid jumps in the magnetic field, speed, density, and temperature (solid vertical line). Using a coplanarity theorem and Rankine-Hugoniot relations [*Abraham-Shrauner and Yun*, 1976, equations (1) and (10)], the Alfvén Mach number of the shock speed was estimated to be 3.8 with the shock angle of 65°. From the statistics of all fast-forward shocks as identified from ACE observations in 1995–2013 (http://ipshoks.fi), the average Alfvén Mach number is only 2.2, and the observed shock is therefore stronger than average, although it is not an exceptionally strong shock. In the shock downstream, a compressed stream interface (SI) [e.g., *Gosling et al.*, 1978] can be identified at 0730 UT by the density drop, speed enhancement, and negative-to-positive change of the $V_y$ component (dash-dotted vertical line). This

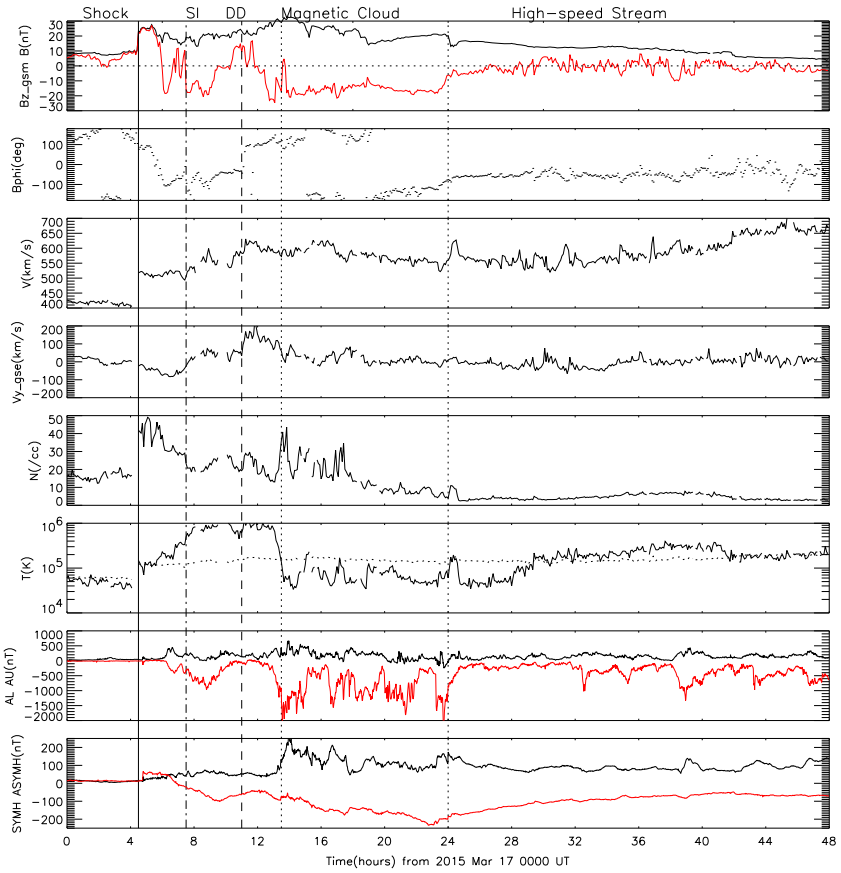


**Figure 1.** Solar wind parameters and geomagnetic activity indices for the 2 day time interval from 17 March 2015. (first to eighth panels) Interplanetary magnetic field strength with the north-south component in GSM coordinate system (red curve), the GSE azimuthal angle, solar wind speed, GSE $V_y$ component, proton density, temperature, *AL* (red curve) and *AU* indices, and *SYM-H* (red curve) and *ASYM-H* indices. The expected temperature [*Lopez*, 1987] is shown by the dotted curve in Figure 1 (sixth panel) to help identify the magnetic cloud. Shock, stream interface, directional discontinuity, and magnetic cloud interval are denoted by solid, dash-dotted, dash, and dotted vertical lines, respectively.

implies that a part of corotating interaction region (CIR) is piled up ahead of the fast CME. In fact, CIRs were observed at corresponding times in previous Carrington rotations, i.e., 27 days and 54 days before (see supporting information). The southward directing interplanetary magnetic field (IMF) embedded in these complex shock downstream structures drove the first step of the storm main phase. The aurora electrojet activity was relatively high already during the sheath passage, up to 1000 nT level as shown in the seventh panel in Figure 1.

Magnetic cloud can be identified by the low temperature against the expected temperature [*Lopez*, 1987], large IMF strength, and relatively smooth rotation of the IMF as shown by the time interval spanned by dotted lines from 1330 UT to 2400 UT. Note that the IMF shows somewhat irregular directional changes during the leading part of the magnetic cloud and that the trailing edge of the magnetic cloud is somewhat ambiguous. The most prominent features of this magnetic cloud are more than a factor of 2 higher-than-average densities and temperatures compared with those of an average magnetic cloud and of average CMEs which caused intense magnetic storms [*Lepping et al.*, 2003; *Kataoka and Miyoshi*, 2006; *Wu et al.*, 2013]. Furthermore, the solar wind speed does not monotonically decrease in the magnetic cloud. Note that the solar wind density is already relatively high up to 20 $cm^{-3}$ preceding the shock and reaches almost 50 $cm^{-3}$ in the sheath region.

In fact, a high-speed stream with a peak velocity of about 700 km/s follows the magnetic cloud. The compression by a high-speed stream has been reported to significantly enhance the geomagnetic response of magnetic clouds with southward magnetic fields in their trailing parts [*Fenrich and Luhmann*, 1998; *Kilpua et al.*, 2012]. The high-speed stream following the CME studied here presumably originates from a large coronal hole, southeast from the flare region, based on the Toward IMF polarity which is consistent with the inward pointing

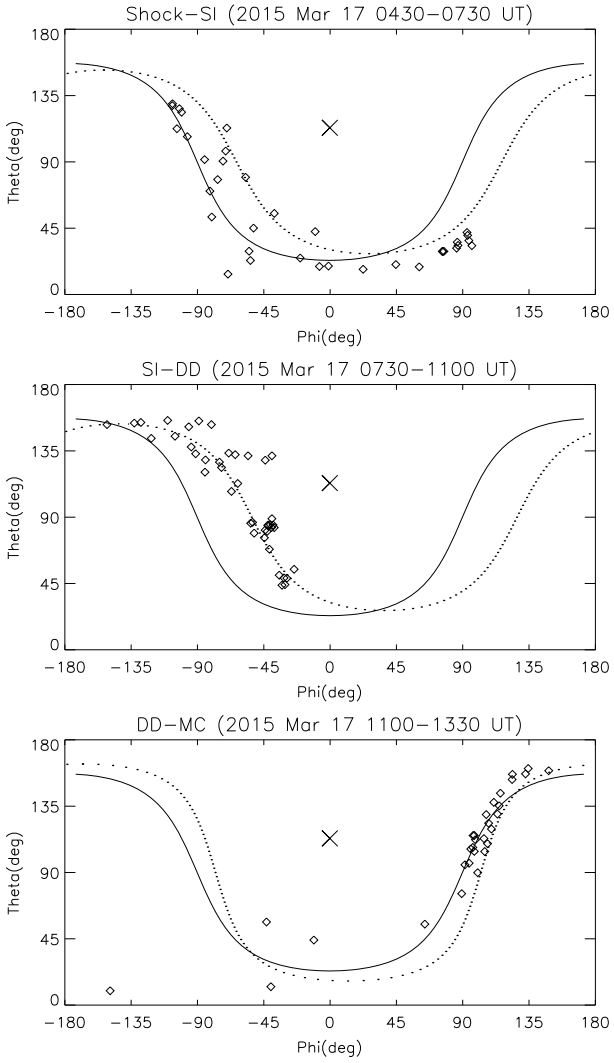


**Figure 2.** Interplanetary magnetic field directions of three identified planar magnetic structures in the sheath region for the time interval from 0430 to 1330 UT on 17 March 2015. Diamonds show the directions of the interplanetary magnetic field in theta and phi GSE spherical coordinate system. The shock normal direction is shown by the cross. Solid curve is the shock plane, and dotted curve shows the fitted plane by the minimum variance analysis for each time interval.

magnetic field of the coronal hole. It is important to note that during the two previous Carrington rotations, CIRs were observed at corresponding times, but with considerably lower peak velocities, only up to 450 km/s (see the solar wind speed profiles in the supporting information). It is therefore likely that the coronal hole structure was changed associated with the fast CME, opening further to the ecliptic and hence enhanced the peak velocity of the CIR and consequently the geoeffectivity of the CME. The coronal holes before and after CME are shown in the supporting information.

## 3. Planar Magnetic Structures

As evidence of "pileup" compression, multiple planar magnetic structures (PMSs) [*Nakagawa et al*., 1989; *Jones et al*., 2002; *Kataoka et al*., 2005] are expected. Figure 2 shows the scatterplots of magnetic field directions in the GSE spherical coordinate system. It is found that there are three PMSs piled up in the sheath region, i.e., from shock to SI, from the SI to directional discontinuity, and from the directional discontinuity to the magnetic cloud front. The shock plane is shown by the solid curve, and the minimum variance plane for each time interval is shown by the dotted curve. All three PMSs have similar orientations, which roughly correspond to the orientation of the shock plane. The normal vectors of the shock plane and of minimum variance planes point slightly southward (theta $>$90°) and sunward (phi ~10–40°, nearly perpendicular to the Parker spiral), which is consistent with the southward CME passage underneath the Earth.

All three PMSs include the southward IMF to drive substorm activities in the first step of the storm main phase as shown in the bottom panels of Figure 1. The first and second PMSs are likely a compression of the CIR (i.e., the shock amplification of the preexisting magnetic fields), while the third PMS is likely associated with the draping of the overlaying solar wind around the CME during its evolution because the magnetic field has similar directions with the following magnetic cloud.

## 4. Simulated Solar Wind Structure

Figure 3 shows the solar wind speed distribution of the background solar wind at equatorial plane and of meridian cut as reproduced by the magnetohydrodynamics simulation of *Shiota et al*. [2014]. It is found that the Earth should be located in the medium speed (~450 km/s) solar wind region just before the fast CME arrives at the Earth.

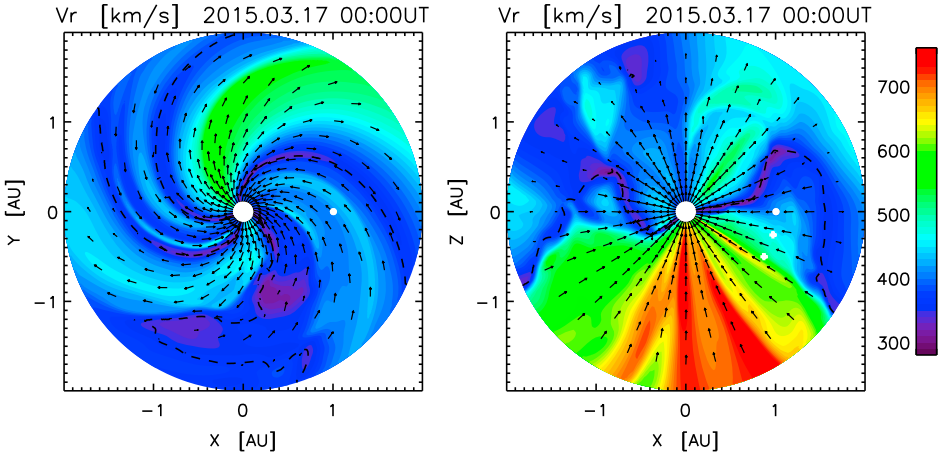


**Figure 3.** Simulated background solar wind in the inner heliosphere. Colors show the speed, and arrows show the direction of the magnetic field. The Earth is located at (*X*, *Y*, *Z*) = (1.0, 0, 0) AU. Virtual Earth positions at 15° and 30° south from equatorial plane are also shown by small white dots.

It is also important to note that the Earth was in the Toward IMF sector in the spring in the Northern Hemisphere as can be predicted from the simulation result. The enhanced southward IMF in the sheath is associated with so-called spring-to-fall away effect [*Russell and McPherron*, 1973]. During the recovery phase, the Earth is again in the Toward IMF sector in spring season in the Northern Hemisphere and then efficiently drives the radiation belt enhancement [*Miyoshi and Kataoka*, 2008, 2011]. Further enhancement of the radiation belt was also expected, since the combination of such CME and high-speed solar wind from nearby coronal hole is the most dangerous solar wind structure as already discussed in *Kataoka and Miyoshi* [2008]. Recently, a combination of a geoeffective sheath and the ejecta, followed by a high-speed stream, was also found as an effective combination to cause relativistic electron enhancements at the geosynchronous orbit [*Kilpua et al.*, 2015].

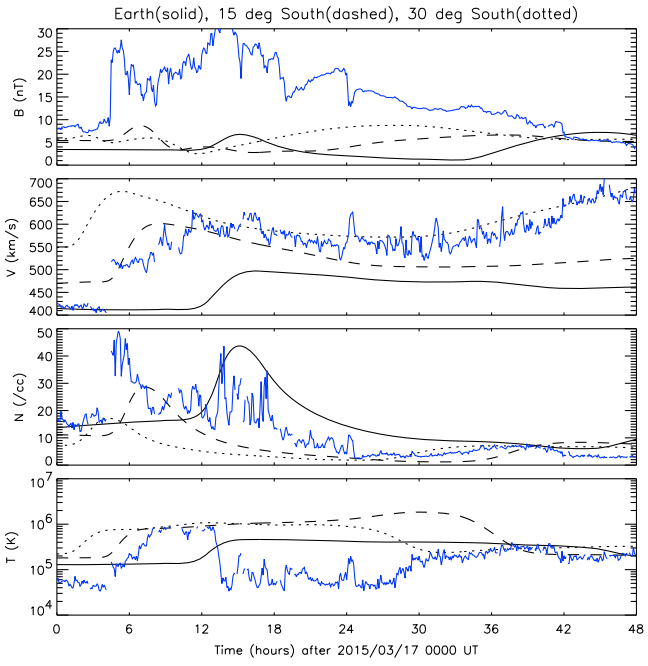


**Figure 4.** Simulated solar wind parameters sampled at the Earth (solid), and at virtual Earth positions of 15° (dashed) and 30° (dotted) southward from the equatorial plane. (first to fourth panels) Magnetic field strength, solar wind speed, density, and temperature for the 2 day time interval from 17 March 2015. The actual observed data are shown by blue curve.

A fast CME is then launched from the flare site into the background solar wind at 0200 UT on 15 March 2015, by the modified method of *Kataoka et al.* [2009]. The spheromak-type magnetic field is initiated at 25 $R_S$ with the axis pointing to the north. The magnetic flux inside is assumed as a typical value ($2 \times 10^{13}$ Wb), and a right-handed magnetic helicity is also assumed. Note that we select these simplest settings to give the reference data, and further detailed modeling is beyond the scope of this paper. The initial speed of the CME is assumed to be 710 km/s as reported by CACTUS (http://sidc.oma.be/cactus/). Figure 4 shows the time profiles of the solar wind parameters sampled at the

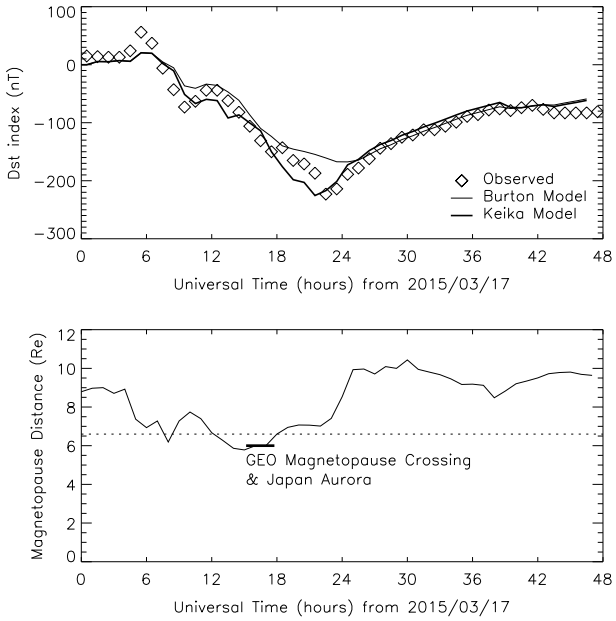


**Figure 5.** Modeled *Dst* index for the 2 day time interval from 17 March 2015 using 1 h averaged solar wind speed, density, and southward IMF in the GSM coordinate system from the OMNI database. Subsolar distance of the magnetopause is also calculated using the same input parameters.

Earth's position. The solar wind profiles at two different virtual Earth positions of 15° and 30° south from the equatorial plane are also shown, to see the propagation effect of the CME through different background solar wind regions. The simulated structure has smaller IMF strength than observed. About a factor of 4 difference of the magnetic field strength still remains as a problem, as was documented in *Shiota et al.* [2014]. However, we avoid further increasing the magnetic field because an unrealistic expansion of the magnetic cloud appears in the current version. The observed high-speed stream following the CME has not been successfully reproduced at the actual Earth's position, which is a modeling issue and remains as important future work. The arrival time of the CME is, however, better estimated for the virtual Earth positions at 15 and 30° south. These locations also show higher peak speed of CIR than what is reproduced at the Earth's position.

To visualize the global context, Movie S1 in the supporting information shows the propagating CME with the same format as Figure 3. The simulation results therefore indirectly help us to visualize and understand the global arrangement of high-speed stream with the IMF sector, slow solar wind, and propagating CME by complementary way against the direct detailed comparisons with the in situ data.

## 5. Geomagnetic Responses

As shown in Figure 5, Burton's *Dst* model [*Burton et al.*, 1975] with O'brien-McPherron's parameter [*O'Brien and McPherron*, 2000] shows a good agreement with the overall two-step evolution with the gradual recovery, while the peak amplitudes of the *Dst* index cannot be reproduced. The modified Burton equation by *Keika et al.* [2015] reasonably reproduces the large peaks. Note that the main difference from the original Burton's model is that Keika's model takes into account the effect of time variation of the solar wind density on the *Dst* index.

The results of the *Dst* modeling presented above highlight the importance of the high density enhancing the ring current and the *Dst* index. As shown in Figure 1, the solar wind density was relatively high throughout this event, especially from the part of the CIR before the shock to the leading part of the magnetic cloud. In particular, large solar wind densities during the northward IMF, which occurred here preceding the shock and in parts of the sheath are associated with dense plasma sheet, which can lead to large ring current intensities [*Terasawa et al.*, 1997; *Lavraud et al.*, 2006; *Farrugia et al.*, 2006].

The timing of the observed geosynchronous magnetopause crossings is also reproduced by Shue's model [*Shue et al.*, 1998]. The strong compression of the magnetosphere at that time may also lead the trapped hot electrons of the inner magnetosphere move farther inward especially at the dawn sector, which contributes to produce the aurora as seen from the Hokkaido, Japan, in the early morning.

## 6. Summary

In summary, the pileup accident hypothesis is proposed for 17 March 2015 storm as follows: First, a fast CME with strong southward magnetic fields both in the sheath and in the ejecta was followed by a high-speed stream from a nearby coronal hole. This combination resulted in less adiabatic expansion than usual to

keep the high speed, strong magnetic field, and high density within the CME. Second, preceding slow and high-density CIR was piled up ahead of the CME just before the arrival at the Earth to further enhance its magnetic field and density. Finally, the enhanced solar wind speed, magnetic field, and density, worked all together to drive the major magnetic storm.

This paper demonstrates an interesting example of how "geoeffective" solar wind structure can be produced during the interplanetary propagation of CMEs. *Kataoka and Miyoshi* [2008] suggested "double rarefaction" mechanism (rarefaction of the solar wind and the magnetosphere) to cause the largest enhancement of the radiation belt electrons, while the new hypothesis proposed in this paper is the "double compression" mechanism (compression of the solar wind and the magnetosphere) to cause large magnetic storms.

A halo CME occurred on 15 March 2015. The CME was followed by a high-speed solar wind stream from a large coronal hole to the southeast of the flare region. The high-speed solar wind continuously pushed the CME from behind during the propagation, and a slow and high-density solar wind was piled up ahead of the CME just before the arrival at the Earth. CIRs with low peak velocities were observed in the previous two Carrington rotations at the corresponding time of the CME arrival. Further, similar CIR related low peak velocity is simulated by magnetohydrodynamics. Hence, the CME eruption likely modified the large-scale coronal structure, rapidly extending the coronal hole open toward the ecliptic and enhancing the peak velocity of the stream and hence significantly contributed to the unexpected geoeffectivity of this event. However, such a dynamical change of the large-scale coronal structure associated with CMEs cannot be captured and forecasted easily by existing solar wind models and therefore an important subject for future space weather forecast. Transiently formed coronal holes are not necessarily filled by high-speed stream, and the observed high-speed stream would give new insight for the fundamental study of the solar wind acceleration mechanism.

A large magnetic storm then occurred on 17 March 2015. The storm main phase had two-step development. The first step was driven by the southward IMF in the sheath region, which is related to the compression of preceding CIR, while the second step was driven by the southward IMF in the magnetic cloud. The solar wind structures are highly compressed in the Toward IMF sector in spring season in the Northern Hemisphere and lead to the unexpectedly large magnetic storm, geosynchronous magnetopause crossing, and aurora observations from Hokkaido, Japan, during the main phase. Consequently, the high-speed coronal hole stream in the Toward IMF sector also caused a large enhancement of radiation belt electrons during the storm recovery phase.

**Acknowledgments**

Solar wind data are obtained from OMNI database (http://omniweb.gsfc.nasa.gov/). *Dst*, *AU*/*AL*, and *SYM-H*/*ASYM-H* indices are obtained from WDC for Geomagnetism, Kyoto University (http://wdc.kugi.kyoto-u.ac.jp/). This paper used data from the Heliospheric Shock Database, generated and maintained at the University of Helsinki. E.K. acknowledges Academy of Finland projects 1218152 and 1267087. This work was supported by JSPS KAKENHI grants 26800255 and 26800257. D.S. and K.K. are supported by the GEMSIS project at STEL/Nagoya University. Part of the work of K.K. was done at the ERG-Science Center operated by ISAS/JAXA and STEL/Nagoya University. The production of this paper was supported by an NIPR publication subsidy.

The Editor thanks Alisson Dal Lago and an anonymous reviewer for their assistance in evaluating this paper.

## References

Abraham-Shrauner, B., and S. H. Yun (1976), Interplanetary shocks seen by AMES plasma probe on Pioneer 6 and 7, *J. Geophys. Res.*, *81*, 2097–2102, doi:10.1029/JA081i013p02097.

Burton, R. K., R. L. McPherron, and C. T. Russell (1975), An empirical relationship between interplanetary conditions and *Dst*, *J. Geophys. Res.*, *80*, 4204–4214, doi:10.1029/JA080i031p04204.

Farrugia, C. J., V. K. Jordanova, M. F. Thomsen, G. Lu, S. W. H. Cowley, and K. W. Ogilvie (2006), A two-ejecta event associated with a two-step geomagnetic storm, *J. Geophys. Res.*, *111*, A11104, doi:10.1029/2006JA011893.

Fenrich, F. R., and J. G. Luhmann (1998), Geomagnetic response to magnetic clouds of different polarity, *Geophys. Res. Lett.*, *25*(15), 2999–3002, doi:10.1029/98GL51180.

Gosling, J. T., J. R. Asbridge, S. J. Bame, and W. C. Feldman (1978), Solar wind stream interfaces, *J. Geophys. Res.*, *83*(A4), 1401–1412, doi:10.1029/JA083iA04p01401.

Jones, G. H., A. Rees, A. Balogh, and R. J. Forsyth (2002), The draping of heliospheric magnetic fields upstream of coronal mass ejecta, *Geophys. Res. Lett.*, *29*(11), 1520, doi:10.1029/2001GL014110.

Kamide, Y., N. Yokoyama, W. Gonzalez, B. T. Tsurutani, I. A. Daglis, A. Brekke, and S. Masuda (1998), Two-step development of geomagnetic storms, *J. Geophys. Res.*, *103*(A4), 6917–6921, doi:10.1029/97JA03337.

Kataoka, R., and Y. Miyoshi (2006), Flux enhancement of radiation belt electrons during geomagnetic storms driven by coronal mass ejections and corotating interaction regions, *Space Weather*, *4*, S09004, doi:10.1029/2005SW000211.

Kataoka, R., and Y. Miyoshi (2008), Magnetosphere inflation during the recovery phase of geomagnetic storms as an excellent magnetic confinement of killer electrons, *Geophys. Res. Lett.*, *35*, L06S09, doi:10.1029/2007GL031842.

Kataoka, R., S. Watari, N. Shimada, H. Shimazu, and K. Marubashi (2005), Downstream structures of interplanetary fast shocks associated with coronal mass ejections, *Geophys. Res. Lett.*, *32*, L12103, doi:10.1029/2005GL022777.

Kataoka, R., T. Ebisuzaki, K. Kusano, D. Shiota, S. Inoue, T. Yamamoto, and M. Tokumaru (2009), Three-dimensional magnetohydrodynamic (MHD) modeling of the solar wind structures associated with 13 December 2006 coronal mass ejection, *J. Geophys. Res.*, *114*, A10102, doi:10.1029/2009JA014167.

Keika, K., Y. Ebihara, and R. Kataoka (2015), What caused the rapid recovery of the Carrington storm?, *Earth Planets Space*, *67*, 65, doi:10.1186/s40623-015-0234-y.

Kilpua, E. K. J., Y. Li, J. G. Luhmann, L. K. Jian, and C. T. Russell (2012), On the relationship between magnetic cloud field polarity and geoeffectiveness, *Ann. Geophys.*, *30*, 1037–1050, doi:10.5194/angeo-30-1037-2012.

Kilpua, E. K. J., H. Hietala, D. L. Turner, H. E. J. Koskinen, T. I. Pulkkinen, J. V. Rodriguez, G. D. Reeves, S. G. Claudepierre, and H. E. Spence (2015), Unraveling the drivers of the storm-time radiation belt response, *Geophys. Res. Lett.*, *42*, 3076–3084, doi:10.1002/2015GL063542.

Lavraud, B., M. F. Thomsen, J. E. Borovsky, M. H. Denton, and T. I. Pulkkinen (2006), Magnetosphere preconditioning under northward IMF: Evidence from the study of coronal mass ejection and corotating interaction region geoeffectiveness, *J. Geophys. Res.*, *111*, A09208, doi:10.1029/2005JA011566.

Lepping, R. P., D. B. Berdichevsky, A. Szabo, C. Arqueros, and A. J. Lazarus (2003), Profile of an average magnetic cloud at 1 AU for the quiet solar phase: Wind observations, *Sol. Phys.*, *212*, 425–444.

Lopez, R. E. (1987), Solar cycle invariance in solar wind proton temperature relationships, *J. Geophys. Res.*, *92*(A10), 11,189–11,194, doi:10.1029/JA092iA10p11189.

Miyoshi, Y., and R. Kataoka (2008), Flux enhancement of the outer radiation belt electrons associated with stream interaction regions, *J. Geophys. Res.*, *113*, A03S09, doi:10.1029/2007JA012506.

Miyoshi, Y., and R. Kataoka (2011), Solar cycle variations of outer radiation belt and solar wind structures, *J. Atmos. Sol. Terr. Phys.*, *73*(1), 77–87, doi:10.1016/j.jastp.2010.09.031.

Nakagawa, T., A. Nishida, and T. Saito (1989), Planar magnetic structures in the solar wind, *J. Geophys. Res.*, *94*(A9), 11,761–11,775, doi:10.1029/JA094iA09p11761.

O'Brien, T. P., and R. L. McPherron (2000), An empirical phase space analysis of ring current dynamics: Solar wind control of injection and decay, *J. Geophys. Res.*, *105*, 7707–7719, doi:10.1029/1998JA000437.

Russell, C. T., and R. L. McPherron (1973), Semiannual variation of geomagnetic activity, *J. Geophys. Res.*, *78*, 92–108, doi:10.1029/JA078i001p00092.

Shiota, D., R. Kataoka, Y. Miyoshi, T. Hara, C. Tao, K. Masunaga, Y. Futaana, and N. Terada (2014), Inner heliosphere MHD modeling system applicable to space weather forecasting for the other planets, *Space Weather*, *12*, 187–204, doi:10.1002/2013SW000989.

Shue, J.-H., et al. (1998), Magnetopause location under extreme solar wind conditions, *J. Geophys. Res.*, *103*(A8), 17,691–17,700, doi:10.1029/98JA01103.

Terasawa, T., et al. (1997), Solar wind control of density and temperature in the near-Earth plasma sheet: WIND/GEOTAIL collaboration, *Geophys. Res. Lett.*, *24*, 935–938, doi:10.1029/96GL04018.

Wu, C.-C., N. Gopalswamy, R. P. Lepping, and S. Yashiro (2013), Characteristics of magnetic clouds and interplanetary coronal mass ejections which cause intense geomagnetic storms, *Terr. Atmos. Ocean. Sci.*, *24*(2), 233–241.